Leaking in history space: A way to analyze systems subjected to arbitrary driving

Bálint Kaszás, Ulrike Feudel, and Tamás Tél

Citation: Chaos **28**, 033612 (2018); doi: 10.1063/1.5013336
View online: https://doi.org/10.1063/1.5013336
View Table of Contents: http://aip.scitation.org/toc/cha/28/3
Published by the American Institute of Physics

Leaking in history space: A way to analyze systems subjected to arbitrary driving

Bálint Kaszás,[1] Ulrike Feudel,[2] and Tamás Tél[1,3]
[1]Institute for Theoretical Physics, Eötvös Loránd University, Pázmány Péter Sétány 1/A, H-1117 Budapest, Hungary
[2]Theoretical Physics/Complex Systems, ICBM, Carl von Ossietzky University Oldenburg, 26129 Oldenburg, Germany
[3]MTA-ELTE Theoretical Physics Research Group, Pázmány Péter Sétány 1/A, H-1117 Budapest, Hungary

(Received 13 November 2017; accepted 28 December 2017; published online 22 March 2018)

Our aim is to unfold phase space structures underlying systems with a drift in their parameters. Such systems are non-autonomous and belong to the class of non-periodically driven systems where the traditional theory of chaos (based e.g., on periodic orbits) does not hold. We demonstrate that even such systems possess an underlying topological horseshoe-like structure at least for a finite period of time. This result is based on a specifically developed method which allows to compute the corresponding time-dependent stable and unstable foliations. These structures can be made visible by prescribing a certain type of *history* for an ensemble of trajectories in phase space and by analyzing the trajectories fulfilling this constraint. The process can be considered as a leaking in history space—a generalization of traditional leaking, a method that has become widespread in traditional chaotic systems, to leaks depending on time. *Published by AIP Publishing.*
https://doi.org/10.1063/1.5013336

A concept ideally suited for the study of dynamical systems with arbitrary time-dependence is that of snapshot attractors[1] (also called pullback attractors in the mathematics and climate-related literature[2–10]). Loosely speaking, a snapshot attractor is an object belonging to a given time instant that is traced out by an *ensemble* of trajectories initialized in a region of the phase space in the past, with all of the ensemble members governed by the same equation of motion. In the dynamical systems community, the concept of snapshot attractors has been known and successfully applied for many years.[11–20] A precursor was the discovery of synchronization by common noise (i.e., by a given realization of a random driving),[21] a case when the snapshot attractor turns out to be regular. The use of deterministic driving goes back to Refs. 6 and 11 and to recent approaches in climate science.[8,19–22] The snapshot view has also been applied to systems with high degrees of freedom[23–27] and to experimental situations.[28,29] The approach proposed in this paper is concentrating on a specific aspect of the dynamics of a non-autonomous dynamical system, which is related to a novel type of leaking manifested as a time-dependent leak in phase space. In other words, we identify sets of trajectories which follow a certain type of history. The related mathematical concept is not that of snapshot attractors, rather, that of snapshot saddles (Ref. 37, Sec. 4.6.1), and their stable and unstable manifolds.

I. INTRODUCTION

In an earlier paper,[30] we studied how chaos dies out in a nonlinear oscillator whose driving amplitude is gradually decreasing, starting from a state governed by a chaotic attractor and ending with a state of rest. We found that small differences in the initial conditions lead to drastic differences over the entire switching off process. Individual trajectories are thus not representative. It was therefore found worth monitoring an ensemble of trajectories that traces out, at any instant of time, a snapshot attractor. As a measure of chaos in such systems, we proposed the use of the variability of the dynamics, expressed as the extension of the snapshot attractor in phase space.

There is a recent interest in finding the conditions under which a snapshot attractor of a system with parameter drift follows, in some sense, the bifurcation diagram of the same system with frozen-in parameters. For systems exhibiting only fixed point attractors, the authors of Refs. 31 and 32 showed that the snapshot attractor may "track" branches of fixed point attractors for slow drifts. "Tracking" can fail, if the drift is too fast[31] or the system possesses folded slow (critical) manifolds in the class of slow-fast systems.[33] Using this language, one of the results of Ref. 30 was that in systems also exhibiting chaotic dynamics, such "tracking" is impossible, the frozen-in fixed point attractors are never similar to the snapshot attractors in the range of non-negligible driving amplitudes. It was also shown that if tracking is possible at all, for small enough rates, then the objects that can be tracked should be the unstable manifolds of transient chaos underlying the frozen-in dynamics. Here, we investigate the same paradigmatic model as in Ref. 30 from the point of view of the underlying phase space structures belonging to certain restrictions in the history space.

In Sec. II, we briefly introduce the model and define the parameters used. We construct the distribution of extinction times, i.e., the time needed for a particular initial condition to stop by using different conditions for stopping (Sec. III). In Sec. IV, a partitioning of initial conditions is presented, based on prescribing the rotational direction of the pendulum over

longer and longer time intervals. As a generalization of traditional leaking,[34] we consider the case of leakings in history space in Sec. V by imposing arbitrary constraints for the histories of the trajectories. The previous examples turn out to be special cases of the general framework. In Sec. VI, we identify the main components of the horseshoe construction known from the theory of transient chaos. We refer them as snapshot saddle, snapshot stable, and unstable manifold. These structures are found to be heavily time-dependent in systems with parameter drifts, a property not present in the case of traditional leakings. We show that these manifolds are parts of the stable and unstable foliations of the original, unleaked problem subjected to parameter drift. Finally, in Sec. VII, we indicate the dependence of the horseshoe structure on the main characteristic of the model, the speed of the parameter drift. We also discuss how leaking in history space is related to the concept of survivability recently proposed in the literature.[35]

II. THE MODEL

We consider, as in Ref. 30, a pendulum with a suspension point periodically oscillating along a horizontal line. The dimensionless equation of motion is as follows:[36]

$$\ddot{\varphi} = -\gamma^2 \sin\varphi - 2\beta\dot{\varphi} + C\cos(\varphi)\cos(t), \tag{1}$$

where φ is the instantaneous angle of the pendulum with respect to the vertical ($\varphi = 0$ in equilibrium). The dimensionless driving period is $T = 2\pi$, while γ represents the dimensionless frequency of the pendulum's small amplitude swingings without driving. The parameter β is a friction constant denoting dissipation. In our numerical study, we fix the values of $\gamma = 1/3$ (the driving frequency is three times that of the eigenfrequency) and of $\beta = 0.05$ (the dissipative relaxation rate is one twentieth of the driving frequency). With dimensionless driving amplitude $C_0 = 2$, i.e., when the amplitude of the suspension point's oscillation is twice as large as the length of the pendulum, the dynamics is chaotic and possesses an underlying chaotic attractor.

The amplitude of the suspension point's oscillation, C, is chosen to be time-dependent, with the following particular exponential "scenario":

$$C(t) = \begin{cases} C_0, & \text{for } t < 0 \\ C_0 \cdot e^{-\alpha \cdot t}, & \text{for } t \geq 0, \end{cases} \tag{2}$$

where α is a constant *switchoff rate*. In the bulk of this paper, we fix $\alpha = 0.025$, a switchoff rate used in the simulations presented in Ref. 30. For visualization of the trajectories, a stroboscopic map is taken, each trajectory is sampled only at integer multiples of the driving period $T = 2\pi$.

Since Eq. (1) represents a typical nonlinear dynamical system with dissipation and Eq. (2) is a representative smooth time dependence of one parameter, the model is expected to exhibit generic features of nonautonomous systems subjected to drifting parameters.

III. DISTRIBUTION OF EXTINCTION TIMES

For the following investigation, we take the chaotic attractor at $C = C_0$ as initial condition, at $t = 0$. To achieve this, we create an ensemble of $N \gg 1$ points and iterate it from $t = -10T$ forward to $t = 0$. We have checked that the attractor is practically reached by this ensemble latest at $t = -7T$.

We numerically determine how much time is needed for the pendulum to "stop" when starting with different initial conditions on the chaotic attractor. Here and in the following phase, space plots are presented in the (φ, $\omega \equiv d\varphi/dt$) plane.

First, we consider a trajectory to have stopped if its phase space distance from the origin is systematically smaller than a threshold value, chosen to be a disk of radius $r = \sqrt{\varphi^2 + \omega^2} = 0.2$. The time instant nT for which this condition is first fulfilled and *kept valid afterwards* is called the extinction time of a given trajectory. The result is shown in Fig. 1. It is surprising that different extinction times might belong to initially neighboring points. Moreover, each color traces out a filamentary structure, whose fibers are more or less perpendicular to that of the attractor. It seems that the extinction dynamics opens up a novel structure underlying the chaotic attractor, but characterizing the full switching off process.

Although the sets are fractal-looking, compact regions of a given color can also be seen, in a pronounced way in red and orange, where these compact regions contain the majority of the points. It is also worth noting that, in contrast to usual chaotic cases, like, e.g., chaotic scattering,[37] the range of the extinction times is rather short, and their distribution is not fractal-like at all as the inset of Fig. 1 illustrates.

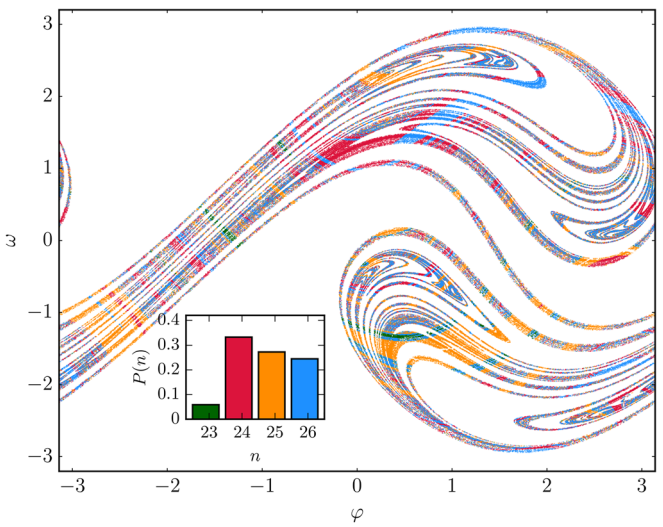

FIG. 1. Distribution of extinction times on the chaotic attractor represented by $N = 2 \times 10^5$ points for a switching off process with $\alpha = 0.025$. The condition for "stopping" is that a trajectory reaches *and* stays afterwards in the disk of radius $r = 0.2$ around the origin. The lifetime is represented by colors, and only those values are shown, to which a considerable number of starting points belong to (more than 5% of the ensemble). The probability distribution $P(n)$ of discrete extinction times (measured in unit of T) can be seen on a bar chart as an inset. The horizontal and vertical axes of this and all the forthcoming phase space plots are the angle φ, and the angular velocity $\omega = \dot{\varphi}$, respectively.

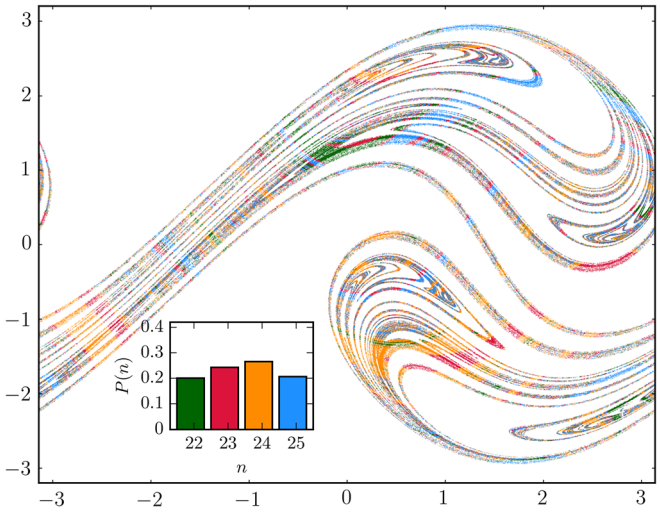

FIG. 2. Distribution of extinction times on the chaotic attractor represented by $N = 2 \times 10^5$ points. $\alpha = 0.025$. The condition for "stopping" is that a trajectory reaches *and* stays in the phase space strip $|\omega| < 0.1$. The probability distribution ($P(n)$) of extinction times can be seen on a bar chart as an inset.

Let us choose a different "stopping" condition. Now, we consider a trajectory to have an extinction time nT if it first reaches the phase space strip $|\omega| < 0.1$ at $t = nT$ and stays in it for $t > nT$. In Fig. 2, we see that an analogous filamentary structure appears as in Fig. 1, with a rather different stopping condition of an area of about 10 times larger than there. The filaments of the different colors seem to run parallel to each other and perpendicular to the attractor, again, but the details differ. Note that the distribution $P(n)$ also differs from that of Fig. 1.

As a next trial, we distribute the initial points (uniformly) over the full rectangle of the phase space $\varphi \in (-\pi, \pi)$ and $\omega \in (-3.2, 3.2)$ shown. Parallel to this, we also consider the extinction times from a cumulative perspective, i.e., we identify points that have an extinction time at most nT. A comparison between the cumulative extinction times and exact extinction times at nT is seen in Fig. 3. Here, the stopping condition is again reaching and staying in the region $|\omega| < 0.1$. To construct the set of trajectories with exactly nT extinction time, one needs to take the difference of two sets: those trajectories that have extinction times at most nT and those that have at most $(n-1)T$. In other words, overlaying the two panels in the left column, one obtains the upper right panel.

In Fig. 4, the initial points of trajectories that have an extinction time exactly nT with $22 \le n \le 25$ are marked by colors. The red and the orange components of the figure are identical to the lower left and lower right panel of Fig. 3, respectively. A similar pattern appears, as in Fig. 2. This is

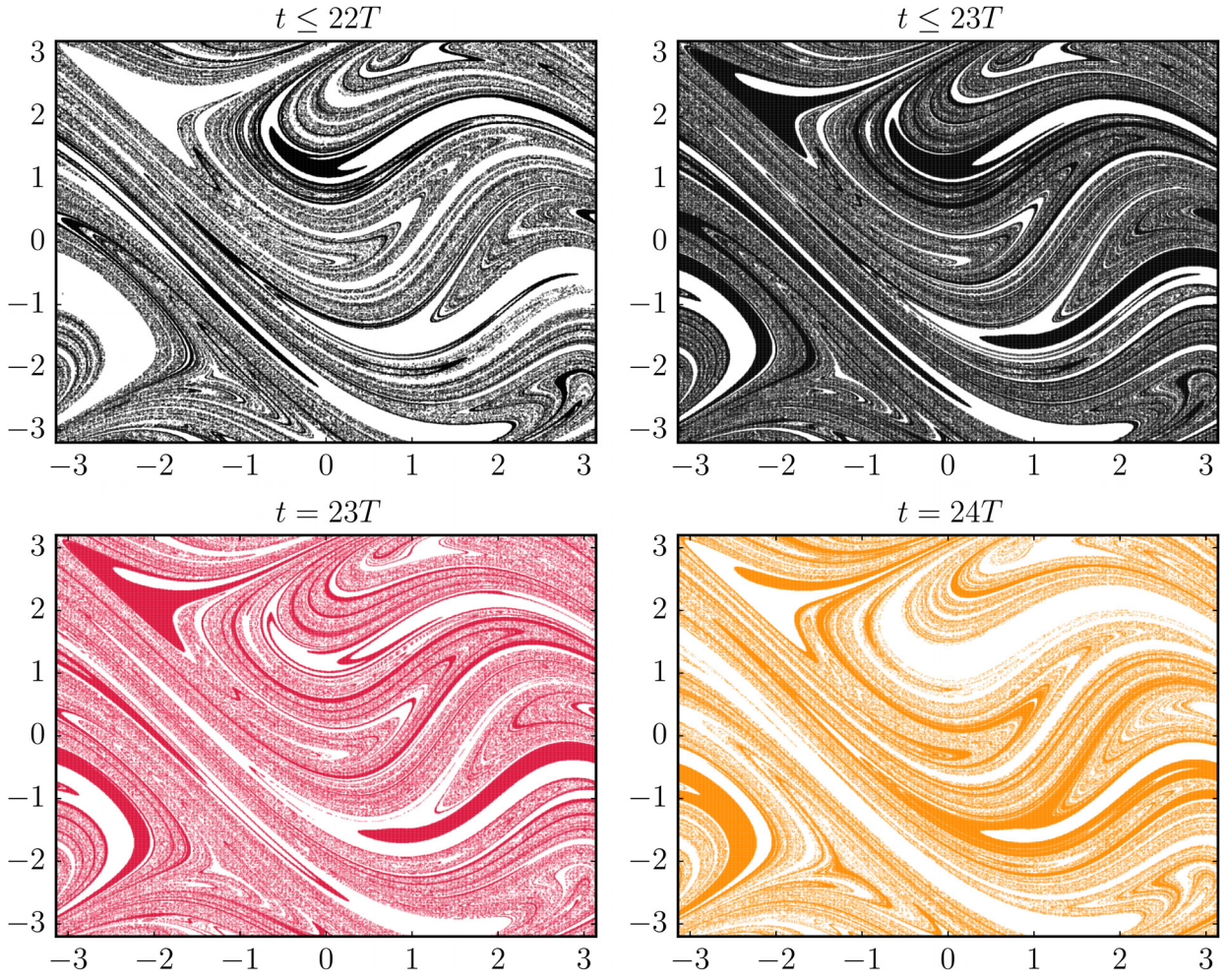

FIG. 3. Distribution of trajectories with extinction times *at most 22 and 23T* (first row) and trajectories with extinction times *exactly 23 and 24T* (second row) over the phase space. The condition for "stopping" is that a trajectory reaches *and* stays in the phase space strip $|\omega| < 0.1$.

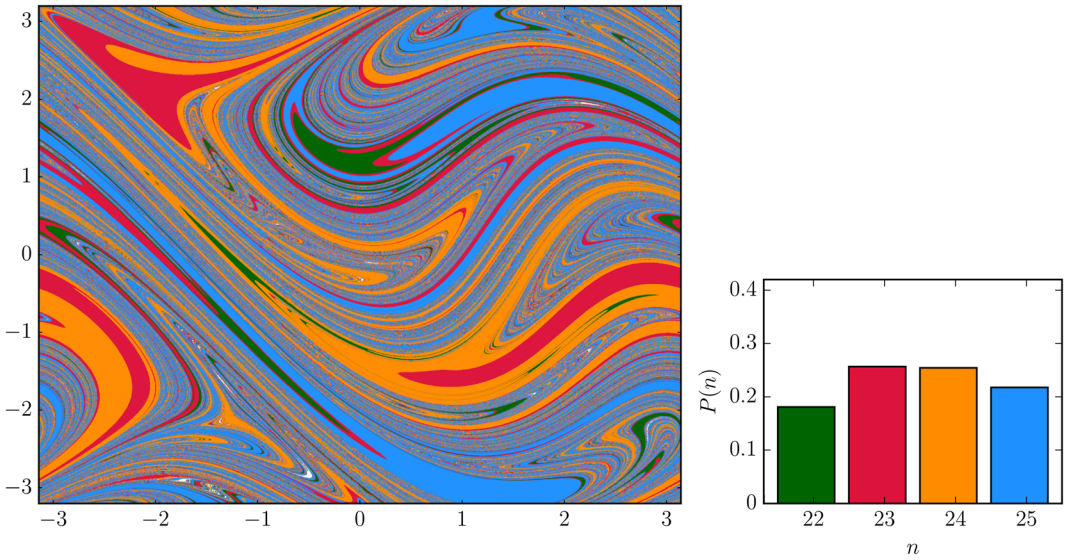

FIG. 4. Distribution of extinction times on the whole phase space region ($\alpha = 0.025$). The condition for "stopping" is that a trajectory reaches *and* stays in the phase space strip $|\omega| < 0.1$. Left panel: extinction times over the phase space, marked by colors. Right panel: probability distribution of extinction times, $P(n)$. Points in the tiny white regions possess an extinction time either less than $22T$ or larger than $25T$.

not surprising, since the initial set chosen now contains the chaotic attractor as a subset. The distribution $P(n)$ of the extinction times is also similar. Figure 2 is nothing but the restriction of Fig. 4 to the chaotic attractor of the case of the $C_0 = 2$ frozen-in driving amplitude.

The prominent extinction times belong to distinct regions of finite area represented with a given color. In certain parts of the phase space, these regions are mixed rather strongly, designated by the appearance of thin filaments, providing an optical appearance similar to that of fractal basin boundaries.[37]

IV. PARTITIONING WITH RESPECT TO THE ROTATIONAL DIRECTION

After having constructed the extinction time distributions, we demonstrate that the emergence of additional filamentary structures specific to the time-dependent process appears to be generic. From here on, instead of partitioning the attractor, we partition the full phase space. We consider a condition different from the extinction time and look for points in the (φ, ω) plane which stay at integer multiples of T, up to a terminal time $t = nT$, in the regions of either $\omega < 0$ or $\omega > 0$, i.e., where the pendulum rotates in a given direction. To generate the partitioning, we first color points according to their ω at time $t = 0$, and then in each period we discard those which change their rotational direction. Figure 5 shows the sequence up to $t = 19T$.

The partitioning is time-dependent. Although between $t = 6T$ and $t = 18T$, no drastic change appears in the ensemble of points, at $t = 19T$, suddenly most of the blue points disappear. The same happens to the red points, but they survive for one more period, and at $t = 20T$ (not shown), they also vanish. There is thus no point, which would rotate all the time in the same direction, since the driving ceases, and dissipation stops the motion.

More generally formulated, we are looking for those points in phase space that have a certain prescribed "history" (in the example of Fig. 5, the constant rotational direction for periods up to t). In this sense, we have constructed the basin for this particular history. For completeness, we present in a supplementary material,[38] the basin for a given sign of the rotation *in continuous time* (not only at integer multiples of T) as a movie. The patterns are similar but shrink faster than in discrete time due to the frequent change of the rotational direction over the first few periods.

The basins in Fig. 5 consist of compact regions in phase space with filamentary looking components as well. In contrast to basins of attraction in usual chaotic systems including periodically driven cases,[37] the basins here are non-periodically time-dependent. The area of the basins shrinks monotonously, with the length of the considered history, and at a threshold value, n_{th} of n suddenly drops to zero. This is a characteristic feature of systems with drifts in their parameters. It is worth noting that the analogous process with a constant amplitude $C_0 = 2$ but with a traditional leak[34] would provide basins that converge to a fractal of zero area, the stable manifold of the chaotic saddle underlying trajectories which rotate in the same direction up to unlimited time.

V. GENERAL LEAKING IN THE HISTORY SPACE

Leaking of traditional chaotic systems means that one defines an artificial leak in the phase space of an originally closed system and investigates the statistics of trajectories leaving the system via the leak. This method opens up a subset of the original phase space structures and can be considered as a tool by which one can look into the details of the original dynamics.[34] Since the condition of entering the leak does not depend on time, this traditional leaking might also be considered as a special leaking in the history space in which no temporal constraint is applied. The concept of

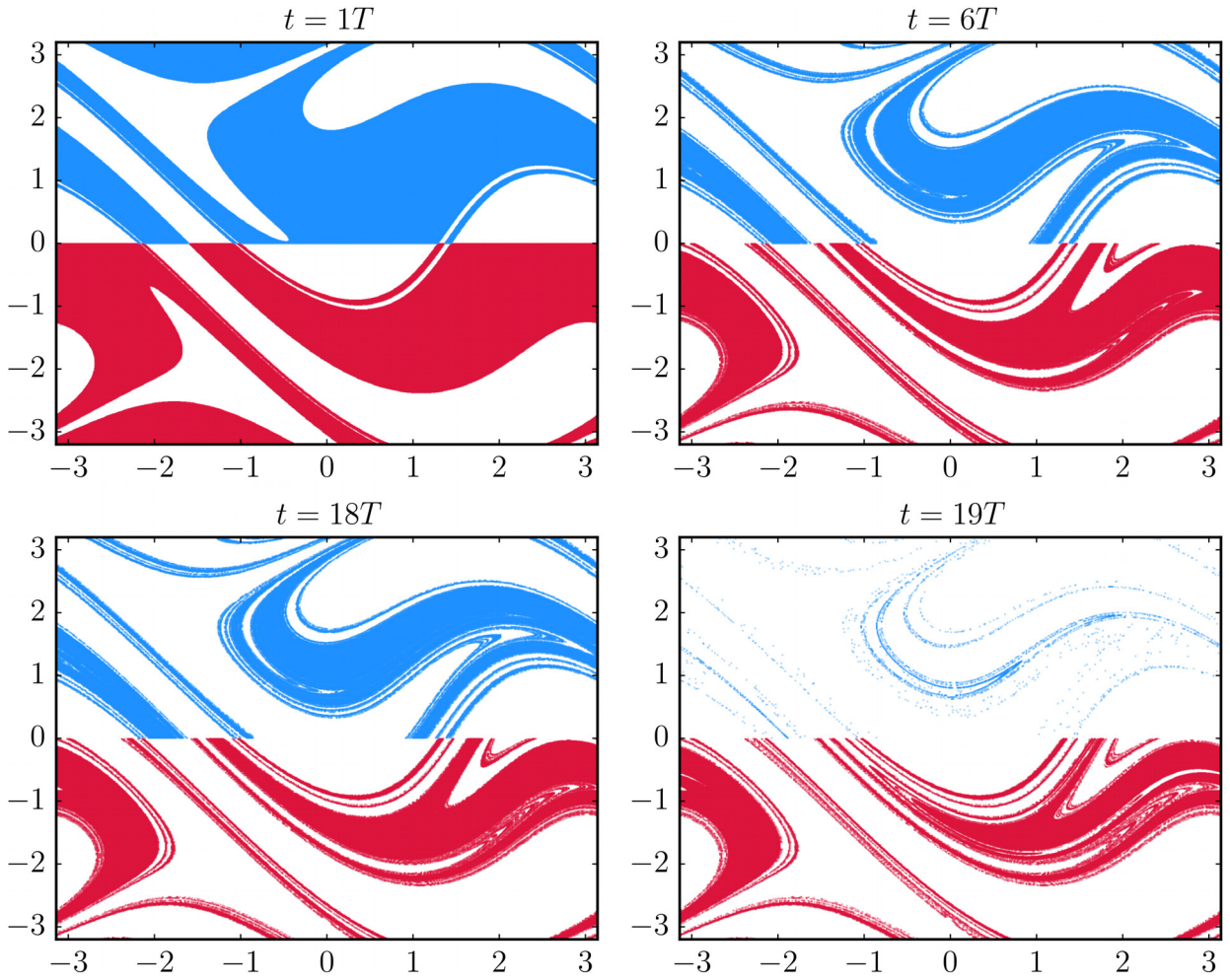

FIG. 5. Partitioning with respect to the trajectories' rotational direction, on the phase-space region shown ($\alpha = 0.025$). Initially, $N = 10^6$ points are distributed uniformly. Blue (red) points correspond to a positive (negative) rotational direction, $\omega > 0$ ($\omega < 0$). In the individual figures, only those points are displayed, which do not change the rotational direction in the stroboscopic map up to time t indicated above the figures.

history space is used here in a similar sense as in the study of dynamical entropies, like e.g., the Kolmogorov-Sinai entropy, in low dimensional ordinary differential equations and maps: we consider the information gained in a series of measurements which follows the coarse grained time development of a system on a given partitioning of the phase space.[39,40] In contrast to these traditional studies, we allow the partitioning to be time-dependent in our setup and this partitioning follows from the constraints used to define the leak in history space. In systems with drifting dynamics, like the decay of the driving in our example, the interest lies in the finite time behavior; therefore, it is rather natural to consider histories prescribed over certain time windows only.

In fact, all of the constraints used up to now can be interpreted as consequences of leaks in the history space. In Figs. 1 and 2, each of the colors represent certain histories which are arbitrary up to time t and end by entering and remaining in a prescribed phase space region. For example, the green foliation in Fig. 2 corresponds to a history which fulfills the condition $|\omega| < 0.1$, for $t \geq 22T$, while the history for red points is similar with $t \geq 23T$. More generally, we can say, that the histories considered in Figs. 1 and 2 are determined by the conditions $\sqrt{\varphi^2 + \omega^2} < 0.2$, $t \geq nT$ with $n = 23,\ldots, 26$ and $|\omega| < 0.1$, $t \geq nT$ with $n = 22,\ldots, 25$, respectively. The leaks in history space can be identified as the complements of histories prescribed in time and phase space. Just like in the case of traditional leaking, whenever a trajectory enters the leak in the history space, it is no longer relevant for the purposes of the observer.

Some leaks in history space can be represented as simple curves on the plane spanned by one of the phase space variables and the time. Figure 6 shows a few examples. For simplicity, we only present here restrictions in the ω coordinate, not in φ or both. In the history representation used, traditional leaking[34] corresponds to defining a forbidden region in phase space, which is independent of time (see inset). The new feature of leaking in history space is that it allows for the time dependence of phase space leaks.

In principle, any history, which lies outside a leak in the history space, can be considered to have a basin.[41] To illustrate general leaks in history space and the basins of the prescribed histories, we consider an asymmetric condition in ω (exemplified by the grey dashed lines in Fig. 6). In the traditional view, these imply applying no leaking up to time $1T$ ($2T$) when suddenly a phase space leak $\omega \notin (0.3, 0.7)$ appears up to time $3T$ ($4T$).

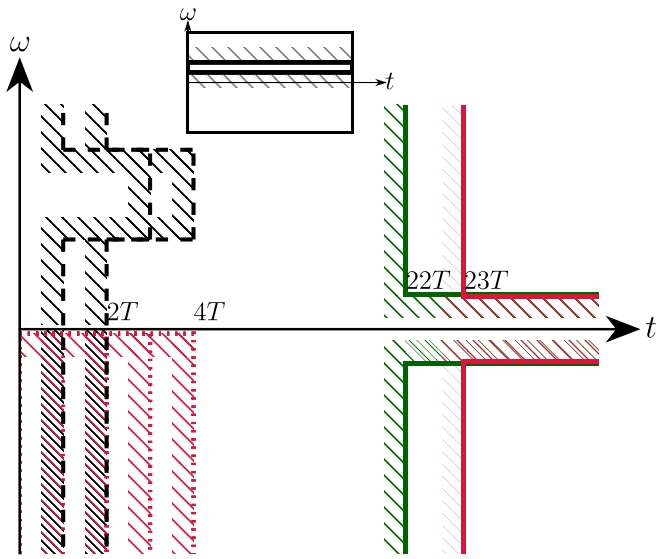

FIG. 6. Schematic diagram of leaks in the history space (not to scale). The regions bounded by colored lines and shaded strips mark different prescribed histories. The complements of these regions, the unshaded regions, are the leaks in history space. In the right part of the figure, the colored lines correspond to the two upper panels of Fig. 3 where the extinction time is $t \le nT$ (for $n = 22$ and 23). The constraints (dotted lines) in the lower left region represent the partitioning condition with respect to the negative rotational direction of Fig. 5, with gradually increasing width along the time axis. The curves in the upper left region (dashed lines) correspond to more general, arbitrarily chosen histories. The feature that these constraints are bounded in time expresses the fact that we consider the dynamics to be irrelevant after the terminating time instant. These particular constraints will be used as further examples in the text. In the inset, an example of a traditional leak represented in the history space is shown.

Figure 7 shows the basin for the history of $0.3 < \omega < 0.7$, $1T \le t \le 3T$, in the right panel, and $2T < t < 4T$, in the left panel. Both patterns are sparser than those of the previous figures at similar times (see, e.g., the first row of Fig. 5), because the prescribed property is much stricter, much less trajectories can satisfy it. To make the structure visible, we had to take an ensemble of much more initial points, than earlier. These structures have the same characteristics as seen before. Mostly, they contain fine filaments and exhibit a clear dependence on the temporal component of the leaking.

Next, we consider two different phase-space constraints in the ω coordinate (Fig. 8), while keeping the time constraint the same as for the right panel of Fig. 7. This implies that these three basins must be disjoint.

A comparison of Figs. 4, 5, 7, and 8 illustrates a general property of leaking in the history space. When comparing the slope of the filaments about a given point [this is especially clear at $(\varphi = -1.5,\ \omega = 1.5)$], we find that the slopes are *almost identical*. The filaments themselves do not necessarily match, but their orientation is the same. This is true despite the histories' different constraints. The conclusion is that in the system under consideration on the plane of initial conditions the slopes about a given point are the same, independent of all the properties of the leaks in history space.[43] Many filaments running parallel to each other in this region also stay similar farther away, as a comparison of the different panels illustrates. In general, leaking in the history space offers the possibility to visualize the filamentation of the dynamics with parameter drift, which is usually dense and therefore not visible without applying any leaking. This observation finally explains the appearance of the striking colored stripes discovered in Figs. 1 and 2 as a kind of stable foliation, more precisely, as the basin of extinction times nT, restricted in these figures to the chaotic attractor.

It is also interesting to investigate how the number of trajectories within the basin of a history depend on time. That is, we measure the number of trajectories which fulfill the condition of being outside a leak, as a function of the terminal point n of the history's temporal component. As an example, we take the phase space constraint used in Figs. 7 and 8 applied in subsequently widening time windows, e.g., $2T \le t \le nT$, with $n = 2, 3, \ldots$, in the left panel of Fig. 7. The result is presented in Fig. 9, where we display the probability of finding a trajectory that satisfies the history $P \approx N/N_0$ vs. n where N is the number of trajectories satisfying the history and N_0 is the number of uniformly distributed initial conditions.

Over the first few steps, the trend appears to be roughly exponential, but later it becomes much faster, the points fall below the dashed lines. The form $\exp(-\kappa n)$ provides thus

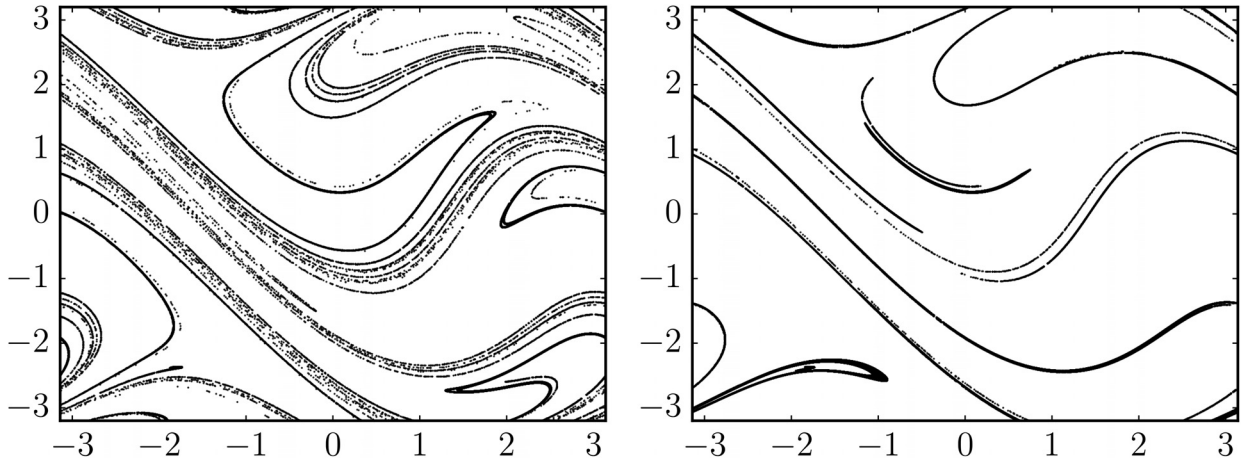

FIG. 7. Basins for staying outside general leaks in the history space. Initially, an ensemble of $N = 10^7$ points is distributed uniformly in phase space for a switching off process with $\alpha = 0.025$. Those points are shown which are in the region $0.3 < \omega < 0.7$ on the stroboscopic map for periods $2T \le t \le 4T$ in the left panel and for periods $1T \le t \le 3T$ in the right panel.

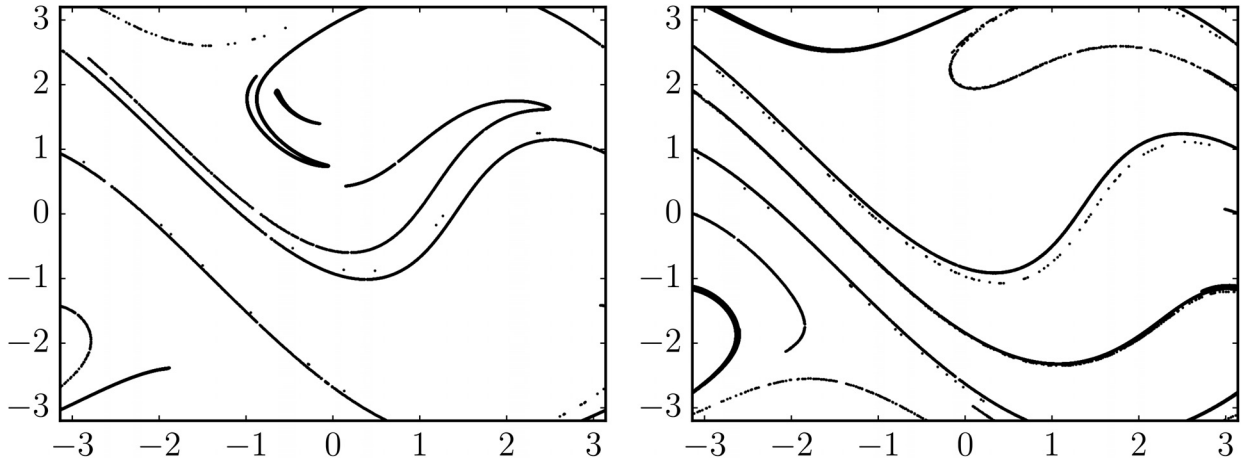

FIG. 8. Basins for staying outside general leaks in the history space, constrained in the same time window. Initially, $N = 4 \times 10^7$ points are distributed uniformly. Left panel: initial position of trajectories that are in the region $0.7 < \omega < 1.1$ (left panel), and in $-0.6 < \omega < -0.2$ (right panel), on the stroboscopic map, for periods $1T \le t \le 3T$, with $\alpha = 0.025$.

an upper bound to $P(n)$. In addition, in all these cases, $N \equiv 0$ beyond a threshold n_{th} (which is on the order of 10 here). Thus, the decay lasts over a finite time interval only. This is in contrast to usual leakings where the exponential behavior $P(n) \sim \exp(-\kappa n)$ holds, in principle, up to unlimited times.

VI. UNDERLYING HORSESHOE-LIKE STRUCTURES

System (1) with frozen-in driving amplitudes C is found to exhibit long-lived transient chaos[37] for a broad range of driving amplitudes (see Fig. 2 of Ref. 30). For fixed C values, this finite-time chaotic dynamics is governed by a nonattracting subset of phase-space, the *chaotic saddle*. The saddle can be approached by trajectories along its *stable manifold*. This is a fractal invariant set of the dynamics, made up of trajectories that converge to the saddle asymptotically. Other trajectories are repelled, along the saddle's *unstable manifold*. This is also a fractal invariant set and consists of trajectories that converge to the saddle in reversed time.

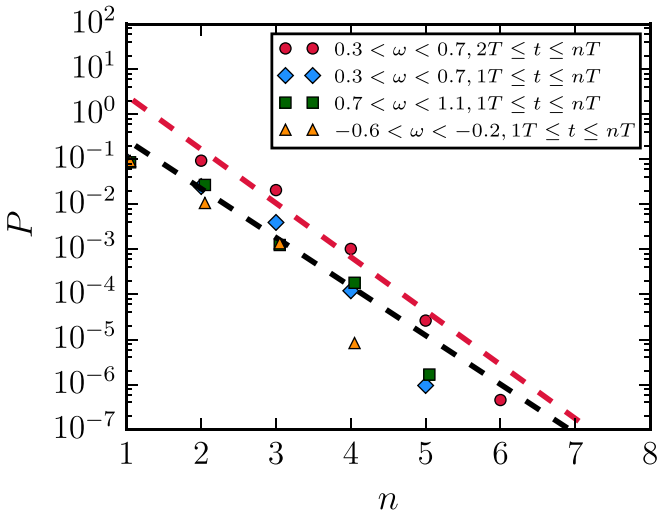

FIG. 9. Probability (P) for a randomly chosen trajectory on the plane of initial conditions to have histories prescribed in Figs. 7 and 8 displayed semi-logarithmically, as a function of the terminating time instant (n) of the history. The different symbols label the histories, while the dashed lines indicate exponential trends (of slopes $\kappa = 2.50$ and 2.75).

It is important to note that the saddle is exactly the intersection of the stable and unstable manifolds. Together with the manifolds, this pattern is referred to as a *horseshoe structure*, the presence of which is known to be a strong indication of chaotic dynamics.[42]

The filamentary patterns seen up to now are reminiscent of manifolds characterizing transient chaos, which might arise due to a traditional leak,[34] i.e., leaks opened forever. Let us, therefore, briefly recall how chaotic saddles and their stable and unstable manifolds are constructed in systems with constant or periodic driving.

In one of the main algorithms (the so-called sprinkler method[37]), one starts with $N_0 \gg 1$ trajectories distributed uniformly over an extended phase space region. One then chooses a time t and follows the time evolution of each initial point up to this time. Only trajectories that do not escape the region outside the leak are kept. If t is sufficiently large (but not too large such that only a few points remain inside), trajectories with a lifetime this long come close to the saddle during the course of their dynamical evolution, implying that their initial points must be in the immediate vicinity of the stable manifold of the saddle (or of the saddle itself), and their end points must be close to the unstable manifold of the saddle. The latter is so because most points still inside after time t are about to leave. The points from the middle of these trajectories (belonging to time $\approx t/2$) are then in the vicinity of the saddle.

For finite values of t, the set of initial points kept, the approximant of the stable manifold, can also be considered to be the basin (possessing a finite area) for the history that the trajectory stays outside the leak for time t. Here, we construct analogous sets of points for the case of decaying amplitude, by choosing leaks in history space.

We consider the case of a given rotational direction and construct the analogues of the stable manifold, the chaotic saddle, and the unstable manifold. These sets, called as

snapshot manifolds and snapshot saddle, are known to be well defined in genuinely open dynamical systems with arbitrary but never vanishing driving.[37]

The results for decaying driving are shown in Fig. 10 for time windows of different length $t = nT$. The prescribed history considered is to have a fixed sign of ω on the stroboscopic map in the time window $(0, t)$. The time window in the last row is only 1 period longer than above, in order to illustrate the drastic change that occurred during the last period to the blue points, as also seen in Fig. 5.

By construction, the snapshot stable manifolds exactly coincide with the basins shown in Fig. 5 but the saddles and the unstable manifolds have not yet been discussed. These sets depend strongly on the time constraint of the prescribed history and can be considered to be snapshot objects. It is the right column here, the snapshot unstable manifold, which is similar in appearance to snapshot attractors, like e.g., the ones found in Ref. 30. The snapshot "saddle" becomes more and more sparse, but exhibits some kind of direct product structure, as usual chaotic saddles do. All of these sets are, of course, of finite area. The unstable manifolds are filamentary, but by times $t = 18T$ or $19T$ they are hardly folded, indicating that the dynamics is, by these long times, no longer chaos-like.

Let us now analyze how these stable and unstable snapshot manifolds look like when we start the decay of the driving not at $C = C_0 = 2$, but at $C = C(4T) = 1.0669$. Figure 11 shows these sets in a different time window which is also of length $18T$. Here, initialization itself takes place at time $t = 4T$ and the investigation ends at $t = 22T$, i.e., the time constraint of the prescribed history is $4T \le t \le 22T$. Even though the time windows have the same length, all the patterns differ considerably from those in the middle row of Fig. 10, a typical property of systems with drifting parameters. Both the stable manifold (the basin for the history) and the saddle are much sparser than in Fig. 10. By taking the plane of initial conditions at a later time, i.e., at $t = 4T$ ($C = 1.0669$), we impose a much stricter non-escape condition since the end of the prescribed time window ($t = 22T$) is at an instant when chaotic motion has nearly stopped. This is

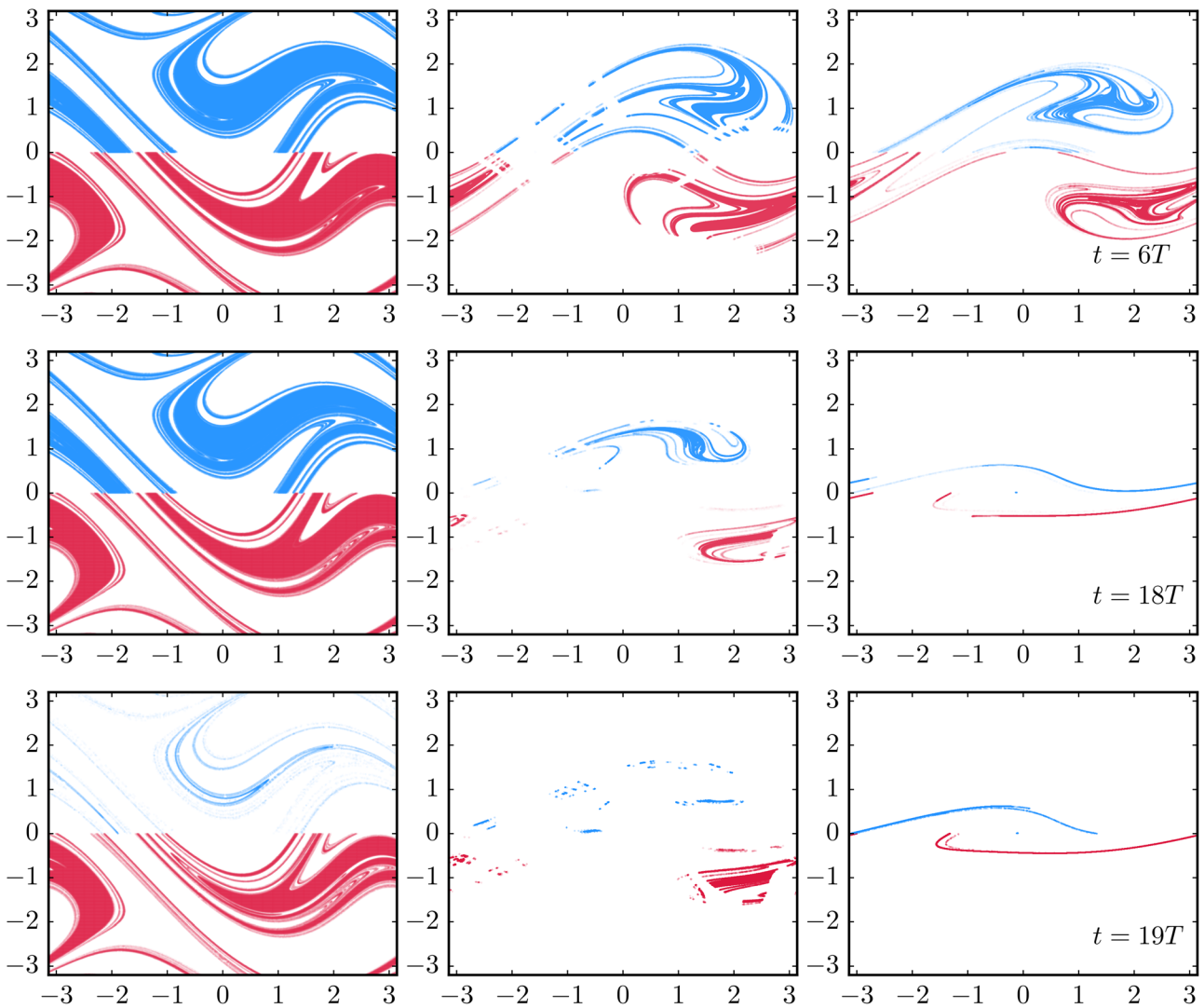

FIG. 10. Snapshot stable manifold (left column), saddle (middle column), and unstable manifold (right column). Red (blue) points represent trajectories with negative (positive) sign of ω up to t on the stroboscopic map, $\alpha = 0.025$. From the top row to bottom, $t = 6T$, $t = 18T$, and $t = 19T$. Stable manifolds are approximated by the trajectories' initial point [$t = 0$], the saddle by their mid-point [at time $\approx t/2$], and unstable manifolds by their endpoint [at time t]. The initial ensemble consisted of $N = 10^6$ points.

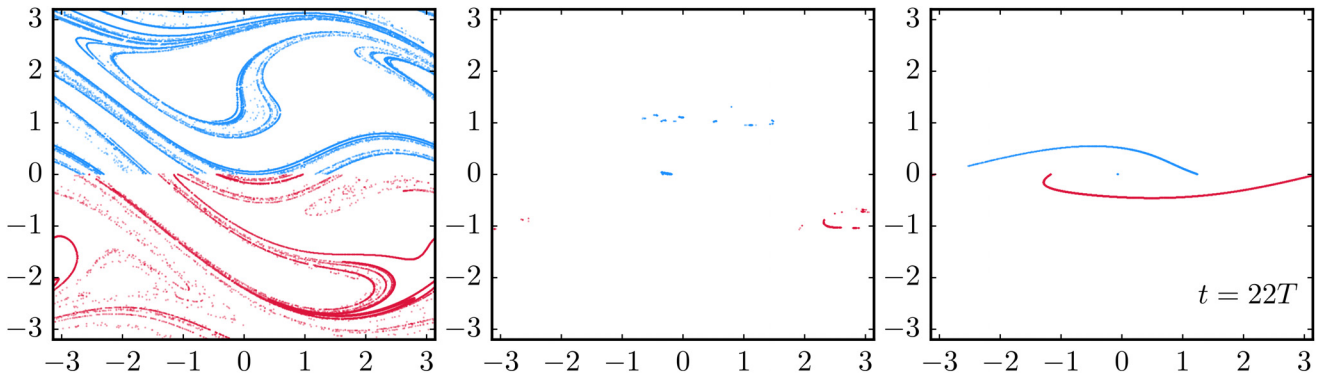

FIG. 11. Snapshot stable manifold (left column), saddle (middle column), and unstable manifold (right column) for a horseshoe-like structure as in Fig. 10, appearing in a time window starting later. Red (blue) points represent trajectories with constant sign of ω for $4T \le t \le 22T$ on the stroboscopic map, $\alpha = 0.025$.

indicated by the fact that the saddle is made up of a few isolated points (or very short intervals) only. The stable foliation of the left panel therefore differs from those of Figs. 4, 5, 7, 8, and 10, which all belong to an initial state with C_0.[44]

The time-dependence of the horseshoe pattern is in strong contrast to cases with persistent time-periodic driving. The latter are exemplified by Fig. 12 where one clearly sees that the increase in the length of the time window from $18T$ to $22T$ only leads to a better convergence to the asymptotic fractal patterns. Here, the number of points fulfilling the non-escape condition decreases exponentially up to long times, with an approximate escape rate $\kappa = 0.28$ for both signs of the rotation (for both the blue and red points).

The chaotic saddle of cases with such traditional leaking does not depend on the temporal part of the leak (time of opening, the length of the time window, provided it is long enough), only on the leak's geometry in phase space. (In this example, the leak for the blue points is $\omega < 0$.)

We thus conclude that in dynamics with parameter drifts the analogues of the stable manifold, of the chaotic saddle, and of the unstable manifold depend on the details of the leak in history space. Nevertheless, a horseshoe-like structure seems to govern the full dynamics, which can be explored by time-dependent leaks.

VII. DISCUSSION

We have shown that generic systems with parameter drift possess a stable and unstable foliation, and an underlying topological horseshoe-like structure, at least for a finite period of time. These structures become visible by prescribing a certain type of history for an ensemble of trajectories in phase space and by analyzing the trajectories fulfilling this constraint. The process is a generalization of traditional leaking to leaks in the history space. This form of leaking might

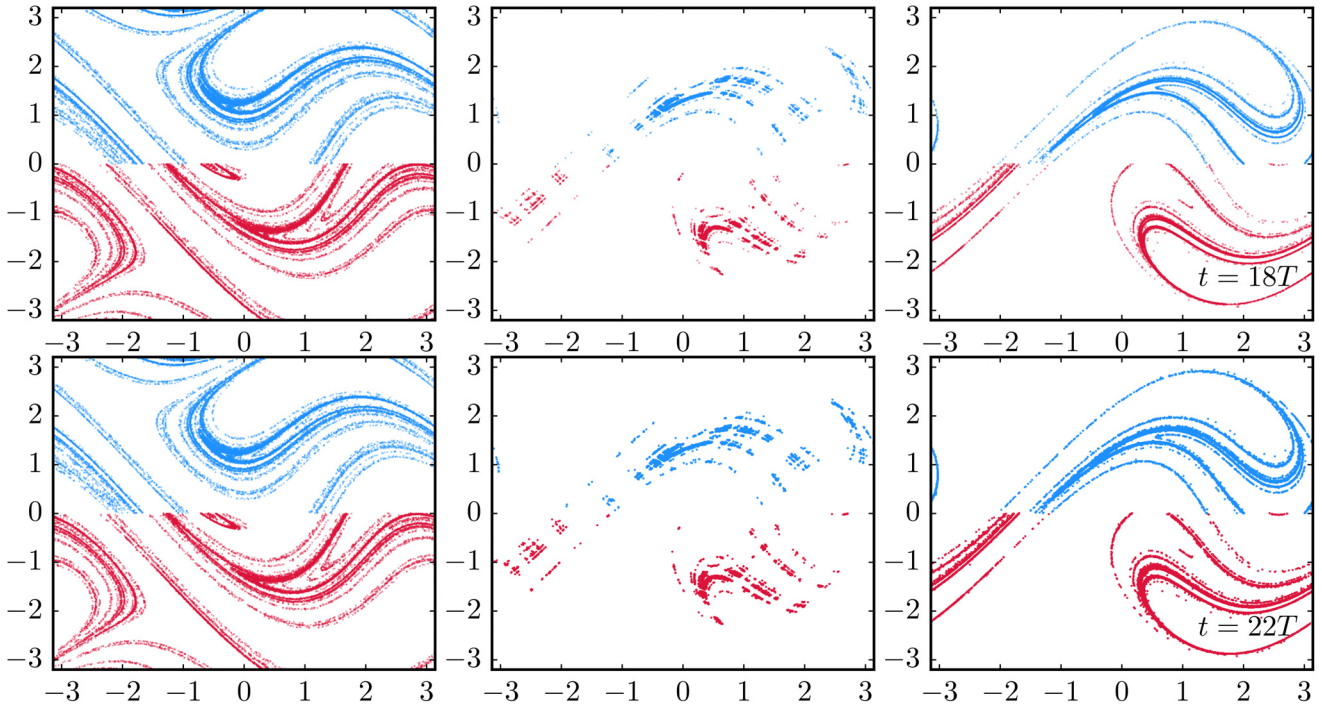

FIG. 12. Stable manifold (left column), saddle (middle column), and unstable manifold (right column) on the stroboscopic map for dynamics with constant $C = C_0$ and $\alpha = 0$. Top (bottom) row shows the horseshoe structure associated with $0 < t < 18T$ ($0 < t < 22T$) and $N_0 = 2 \times 10^5$ ($N_0 = 10^7$). There is practically no dependence on the length of the time window.

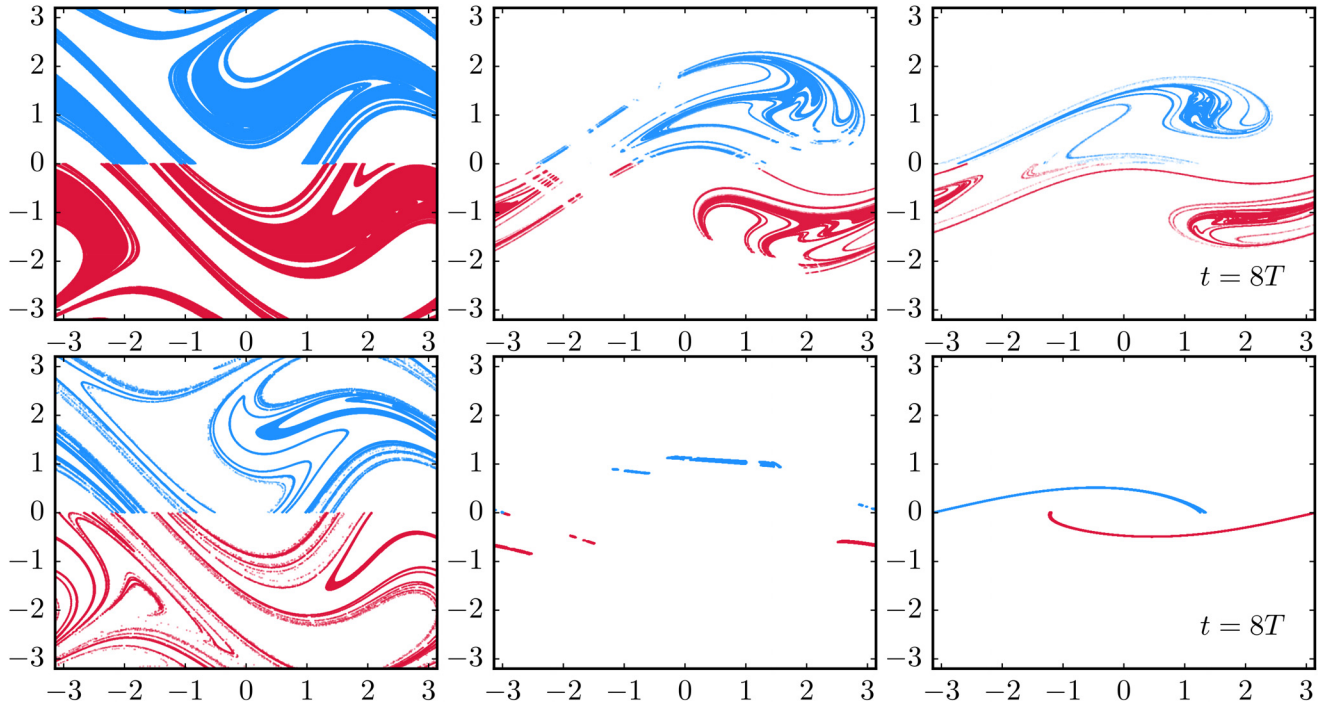

FIG. 13. Snapshot stable manifold (left column), saddle (middle column), and unstable manifold (right column) for a leak provided by the constancy of the sign of ω in the time window $0 < t < 8T$ with switchoff rate $\alpha = 0.025$ (top) and $\alpha = 0.1$ (bottom).

become a method for a detailed analysis of dynamics driven by arbitrarily time dependent forcings.

After having seen that the "chaotic sets" depend essentially on the structure of the leak in history space, we briefly turn now to the dependence on the speed of the drift. Throughout the text, we used the switchoff rate $\alpha = 0.025$, which is less than the rate of dissipation, $\beta = 0.05$. Now, we compare it to $\alpha = 0.1$, which corresponds to a much faster scenario.

Figure 13 suggests a strong dependence of the horseshoe structures on the switchoff rate. With a faster scenario, the chaotic set is much sparser; the unstable manifold is much less folded indicating that chaos-like features disappear faster.

In Ref. 35, the concept of survivability was introduced. Similarly to our problem, a subset of phase space is declared to be *safe*, in the sense that the trajectories of interest are those that never leave this region when starting with a uniform initial distribution in the phase space. This appears to be a generalization of the concept of a "tolerable window" introduced much earlier in the context of climate research.[45,46] There, after specifying the desired region of phase space, the tolerable trajectories are computed backwards. Moreover, the constraint of the tolerable window is prescribed in one of the variables (in a projection of the phase space), while in Ref. 35 the full phase space is taken into account. The conditions in phase space considered in Ref. 35 are independent of time. The system's survivability $S(t)$ is then defined to be the number of trajectories that stay in the safe region up to time t. This concept is similar to traditional leaking, just the observation time is allowed to be finite. Among our examples, Fig. 5 and the dotted curves in the lower left part of the schematics of Fig. 6 also correspond to this concept. By contrast, in our general setup, we let the safe region be an arbitrarily prescribed history, the complement of which is the leak in the history space. We can extend and generalize the concept of survivability to such cases to be the number of initial conditions that obey a prescribed *history* in a certain time interval. Thus, e.g., the PDF $P(n)$ given in the inset of Figs. 1, 2, and 4 (n being a discrete time) can be considered as examples of such generalized survivabilities.

Survivability is defined in Ref. 35 for systems of arbitrary dimensions. Our aim has been the exploration of the phase space patterns related to survivability in low-dimensional problems, and an extension of the concept of leaking. In particular, we investigated the phase space geometry of the basin of history (basin of survival), i.e., the region in which the condition of survival is fulfilled, for a finite amount of time at least, and found that such a basin typically contains a filamentary structure, if the underlying deterministic dynamics involves transient chaos. The authors of Ref. 35 consider survivability conditions applied from time zero up to arbitrarily long times. We have shown that the survivability conditions do not need to be time-independent and can be applied in finite time windows starting at any time instants, implying a general leaking in the history space. This extension allowed us to find the analogue of a horseshoe construction for any drifting dynamics, for which the finite time analogues of saddles, unstable and stable manifolds can be constructed, shedding light on the filamentation of the original, unleaked problem with parameter drift.

ACKNOWLEDGMENTS

We benefited from useful discussions with G. Drótos and C. Kuehn. T.T. is grateful for the support from the Alexander von Humboldt Foundation. This work was also supported by the Hungarian Science Foundation under Grant

No. K 125171. U.F. is grateful for the support from the Hungarian Academy of Sciences.

[1]F. J. Romeiras, C. Grebogi, and E. Ott, Phys. Rev. A **41**, 784 (1990).
[2]H. Crauel, A. Debussche, and F. Flandoli, J Dyn. Differ. Eq. **9**, 307 (1997).
[3]L. Arnold, *Random Dynamical Systems* (Springer, New York, 1998).
[4]M. Ghil, M. D. Chekroun, and E. Simonnet, Physica D **237**, 2111 (2008).
[5]M. D. Chekroun, E. Simonnet, and M. Ghil, Physica D **240**, 1685 (2011).
[6]P. Kloeden and M. Rasmussen, *Nonautonomous Dynamical Systems*, Mathematical Surveys and Monographs Vol. 176 (American Mathematical Society, 2011).
[7]T. Bódai and T. Tél, Chaos **22**, 023110 (2012).
[8]G. Drótos, T. Bódai, and T. Tél, J. Clim. **28**, 3275 (2015).
[9]A. N. Carvalho, J. A. Langa, and J. C. Robinson, *Attractors for Infinite-Dimensional Nonautonomous Dynamical Systems*, Applied Mathematical Sciences Vol. 182 (Springer, New York, 2013).
[10]T. Nishikawa and E. Ott, Chaos **24**, 033107 (2014).
[11]L. Yu, E. Ott, and Q. Chen, Phys. Rev. Lett. **65**, 2935 (1990); Physica D **53**, 102 (1991).
[12]J. C. Sommerer and E. Ott, Science **259**, 335 (1993).
[13]Y.-C. Lai, U. Feudel, and C. Grebogi, Phys. Rev. E **54**, 6070 (1996).
[14]J. Jacobs, E. Ott, T. Antonsen, and J. Yorke, Physica D **110**, 1 (1997).
[15]Z. Neufeld and T. Tél, Phys. Rev. E **57**, 2832 (1998).
[16]J. L. Hansen and T. Bohr, Physica D **118**, 40 (1998).
[17]G. Károlyi, T. Tél, A. P. S. de Moura, and C. Grebogi, Phys. Rev. Lett. **92**, 174101 (2004).
[18]R. Serquina, Y.-C. Lai, and Q. Chen, Phys. Rev. E **77**, 026208 (2008).
[19]T. Bódai, G. Károlyi, and T. Tél, Phys. Rev. E **83**, 046201 (2011).
[20]A. Hadjighasem, M. Farazmand, and G. Haller, Nonlinear Dyn. **73**, 689 (2013).
[21]A. Pikovsky, in *Nonlinear and Turbulent Processes in Physics*, edited by R. Z. Sagdeev (Harwood Academic Publishers, Reading, 1984), Vol. 3; Radiophys. Quantum Electron. **27**, 576 (1984).
[22]J. D. Daron and D. A. Stainforth, Environ. Res. Lett. **8**, 034021 (2013); Chaos **25**, 043103 (2015).
[23]W. L. Ku, M. Girvan, and E. Ott, Chaos **25**, 123122 (2015).
[24]M. Herein, J. Márfy, G. Drótos, and T. Tél, J. Clim. **29**, 259 (2016).
[25]S. Pierini, M. Ghil, and M. Chekroun, J. Clim. **29**, 4185 (2016).
[26]M. Herein, G. Drótos, T. Haszpra, J. Márfy, and T. Tél, Sci. Rep. **7**, 44529 (2017).
[27]M. Herein, G. Drótos, T. Bódai, F. Lunkeit, and V. Lucarini, "Reconsidering the relationship of the El Niño–Southern Oscillation and the Indian monsoon using ensembles instate-of-the-art Earth system models," preprint (2018).
[28]M. Vincze, "Modeling climate change in the laboratory," in *Teaching Physics Innovatively*, edited by A. Király and T. Tél (Ph.D. School of Physics, Eötvös University, Budapest, 2016), pp. 107–118.
[29]M. Vincze, I. Borcia, and U. Harlander, Sci. Rep. **7**, 254 (2017).
[30]B. Kaszás, U. Feudel, and T. Tél, Phys. Rev. E **94**, 062221 (2016).
[31]P. Ashwin, S. Wieczorek, R. Vitolo, and P. Cox, Philos. Trans. R. Soc. London, Ser. A **370**, 1166 (2012).
[32]P. Ashwin, C. Perryman, and S. Wieczorek, Nonlinearity **30**, 2185–2210 (2017).
[33]S. Wieczorek, P. Ashwin, C. M. Luke, and P. M. Cox, Proc. R. Soc. A **467**, 1243 (2011).
[34]E. G. Altmann, J. S. E. Portela, and T. Tél, Rev. Mod. Phys. **85**, 869–918 (2013).
[35]F. Hellmann, P. Schultz, C. Grabow, J. Heitzig, and J. Kurths, Sci. Rep. **6**, 29654 (2016).
[36]T. Tél and M. Gruiz, *Chaotic Dynamics* (Cambridge University Press, Cambridge, 2006).
[37]Y.-C. Lai and T. Tél, *Transient Chaos* (Springer, New York, 2011).
[38]In the following animation, the time evolution of an ensemble of trajectories is shown (black points with an initially uniform distribution) for dynamics (1) and (2) with $\alpha = 0.025$. The blue and red points indicate those trajectories at time t within the ensemble that do not change their sign of ω over the time interval $(0T; 4T]$.
[39]A. Csordás and P. Szépfalusy, Phys. Rev. A **39**, 4767–4777 (1989).
[40]J. D. Farmer, Z. Naturforsch. A **37**, 1304–1325 (1982).
[41]These basins might be empty, if, e.g., the constraints contradict basic features of the dynamics.
[42]E. Ott, *Chaos in Dynamical Systems* (Cambridge University Press, 1993).
[43]Note that this only holds for the stable foliation and for dynamics started at the same time. The unstable foliation is strongly time-dependent (see Sec. VI).
[44]To unfold the unstable foliation, one should consider time windows which *end* at the same time.
[45]G. W. Yohe, Global Environ. Change **7**, 303–315 (1997).
[46]G. Petschel-Held, H.-J. Schellnhuber, T. Bruckner, F. L. Tóth, and K. Hasselmann, Clim. Change **41**, 303–331 (1999).